

Comparative Study of Ethylene Carbonate-Based Electrolyte Decomposition at Li, Ca, and Al Anode Interfaces

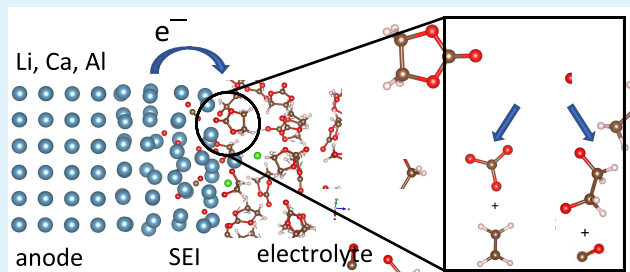
Joshua Young,*¹ Peter M. Kulick, Taylor R. Juran, and Manuel Smeu*¹

Department of Physics, Binghamton University, Binghamton, New York 13902, United States

Supporting Information

ABSTRACT: One of the major bottlenecks to the development of alternatives to existing Li ion battery technology, such as Li metal or multivalent ion (Mg, Ca, Zn, or Al) batteries, has to do with the layer of inorganic and organic compounds that forms at the interface between the metallic anode and electrolyte via solvent and salt decomposition (the solid–electrolyte interphase or SEI). In Li metal batteries the growth of dendrites causes continual formation of new SEI, while in multivalent ion batteries the SEI does not allow for the diffusion of the ions. Finding appropriate electrolytes for such systems and gaining an understanding of SEI formation is therefore critical to the development of secondary Li metal and multivalent ion cells. In this work, we use *ab initio* molecular dynamics simulations to investigate the initial stages of decomposition of organic electrolytes based on ethylene carbonate (EC) and formation of the SEI on Li, Ca, and Al metal surfaces. We first find that pure EC only decomposes to CO and C₂H₄O₂^{2−} species on each type of surface. However, when a salt molecule is introduced to form an electrolyte, a second EC decomposition route resulting in the formation of CO₃^{2−} and C₂H₄ begins to occur; furthermore, a variety of different inorganic compounds, depending on the chemical composition of the salt, form on the surfaces. Finally, we find that EC breaks down more quickly on Li and Ca surfaces than on Al and show that this is because the rate of charge transfer is much faster owing to their lower electronegativity and ionization energies. The molecular level understanding of decomposition and SEI formation generated by this computational modeling can lead to the design of new electrolytes for beyond-Li ion batteries.

KEYWORDS: batteries, multivalent ion, electrolyte, solid–electrolyte interphase, molecular dynamics, density functional theory



1. INTRODUCTION

Energy storage is one of the most important issues of the modern era, as it is key to the widespread implementation of renewable sources such as solar and wind; because these sources are intermittent, secondary (rechargeable) batteries are needed to provide electricity when sunlight or wind is not present.¹ To this end, large arrays of inexpensive electrochemical cells are required for the grid-based storage required to store this energy.^{2,3} Currently, Li ion batteries using graphitic anodes dominate the secondary battery market,⁴ but concerns with cost, safety, and terminal energy density have inspired scientists to look elsewhere for solutions to this problem.^{5–8} For example, one route is to replace graphite with Li metal as the anode, which improves the theoretical capacity nearly 10-fold;^{9,10} however, the growth of dendrites when plating Li metal presents a challenge (although recent work has made significant progress in overcoming this).¹¹ Multivalent ion batteries (MVBs, or those using ions such as Mg²⁺, Ca²⁺, Zn²⁺, or Al³⁺) are also gaining increasing attention due to the fact that they use earth-abundant (i.e., inexpensive) elements and are able to provide multiple electrons per atom.^{12–20} However, one of the major challenges in the adoption of these alternative technologies is the discovery of compatible

electrolytes with metallic anodes, the use of which would greatly increase the capabilities of such systems.^{21–23}

The decomposition of the electrolyte (typically LiPF₆ salt in a solvent of ethylene carbonate [EC] and propylene carbonate [PC] in current Li ion battery technologies²⁴) at the interface with the anode, occurring when the electrochemical window of the electrolyte is outside of the electrode redox potential,²⁵ forms a passivating layer of inorganic (close to the anode) and organic (far from the anode) compounds called the solid–electrolyte interphase (SEI).^{26–29} The SEI is electrically insulating but allows for the diffusion of Li ions and provides a multitude of beneficial properties, such as preventing additional electrolyte decomposition, imparting stability to the anode, and preventing solvent intercalation (however, we note that it also increases in the interfacial resistance).^{30–32} However, in batteries such as Li–air or Li–S, which use Li metal as an anode, the continual change in the surface morphology driven by dendrite formation means that SEI formation does not stop.^{10,33} In multivalent ion batteries such as those using Ca, one major problem is that the SEI forms but

Received: October 7, 2018

Accepted: February 19, 2019

Published: February 19, 2019

does not allow for the diffusion of ions or efficient plating and stripping of the metal anode.^{12,34,35} Recently, Ponrouch et al. showed that electrolytes consisting of an EC/PC solvent and a $\text{Ca}(\text{ClO}_4)_2$ salt allows for the plating of Ca but produces ionically insulating compounds such as CaF_2 .³⁶ Wang et al. then found that $\text{Ca}(\text{BH}_4)_2$ in tetrahydrofuran (THF) forms a layer of CaH_2 which allows for Ca stripping and plating, but with too low of an efficiency for practical use.³⁷ In Al ion batteries, ionic liquids are often used as the electrolyte solvent since nonaqueous organic solvents suffer from several similar problems as in Ca ion batteries, including low solubilities of Al salts, low Al plating and stripping efficiencies, and formation of ionically insulating species such as AlF_3 ;^{38–43} however, ionic liquids suffer from their own drawbacks, including prohibitive costs and high viscosities.^{14,44}

As this shows, studying the interactions between different electrolytes and anodes is critical to improving these alternatives to current Li ion battery technology. By understanding how electrolytes decompose and form different inorganic and organic SEI components, it can be possible to consider new electrolytes that can avoid certain ionically insulating compounds.^{45,46} In this work, we investigate the initial phases of ethylene carbonate (EC)-based electrolyte decomposition and SEI formation on Li (monovalent), Ca (divalent), and Al (trivalent) anodes using *ab initio* molecular dynamics calculations. By considering this series of metal surfaces we are able to determine chemical trends and study a variety of different interfaces; the reactions will differ owing to the fact that these calculations are performed on different pure metal surfaces without an applied external potential.

Because we are studying electrolyte decomposition on pure metal surfaces, we first find that, while EC decomposition occurs quickly on Li and Ca metal, it happens much more slowly on an Al surface. Moreover, there are two routes through which EC can decompose; we find that only one occurs in pure EC, while both routes occur only when a salt molecule is present. Finally, we find a variety of different inorganic compounds on each surface depending on the salt present in the electrolyte.

2. METHODS

These *ab initio* molecular dynamics⁴⁷ calculations were performed using density functional theory^{48,49} as implemented in the Vienna *ab initio* Simulation Package (VASP)^{50–52} using projector augmented wave (PAW) potentials⁵³ and the PBE exchange-correlation functional.⁵⁴ All calculations utilized a 500 eV plane wave cutoff. A $3 \times 2 \times 6$ repetition of a Li, Ca, or Al unit cell was used to construct a 6-layer [001]-terminated metal surface. We first inserted 30 molecules of ethylene carbonate above this surface, the initial configuration of which was created using the PACKMOL software⁵⁵ and quenched using density functional forces. We then replaced one molecule of ethylene carbonate with a molecule of LiPF_6 , $\text{Ca}(\text{PF}_6)_2$, or AlCl_3 , as well as one system where two molecules of ethylene carbonate were replaced with two molecules of AlCl_3 . A 10 ps *ab initio* molecular dynamics (AIMD) trajectory was performed for each at both 350 and 450 K using a Nosé thermostat with a time step of 1 fs (using a tritium mass for hydrogen atoms); only the Γ *k*-point was used in these calculations. Postprocessing was performed using an in-house Python script that determines how many ethylene carbonate rings are broken as a function of simulation time. It does this by using the distance formula(s) to monitor bond lengths between C and O atoms, while also accounting for periodic boundary conditions. The script also determines when these EC molecules decomposed, what products are formed, and the position and angle (with respect to the *a*, *b*, and *c* crystallographic axes) at which the EC rings broke. To

compute the Bader charges we performed a self-consistent calculation on the atomic configuration every 100 fs; the Bader charges were then computed using postprocessing tools developed by Henkelman et al.^{56–59}

3. RESULTS

To understand how EC-based electrolytes decompose, we investigated pure EC and an EC/ LiPF_6 electrolyte on Li metal, an EC/ $\text{Ca}(\text{PF}_6)_2$ electrolyte on Ca metal, and pure EC and two different EC/ AlCl_3 electrolytes on Al metal; each simulation was performed at 350 and 450 K for a total of 12 simulations. We considered pure EC and EC/ $\text{Ca}(\text{ClO}_4)_2$ electrolyte on Ca metal in a previous work.²⁰ Previous studies have identified two different two-electron decomposition routes EC can undergo, as summarized in Figure 1.^{60–67} The

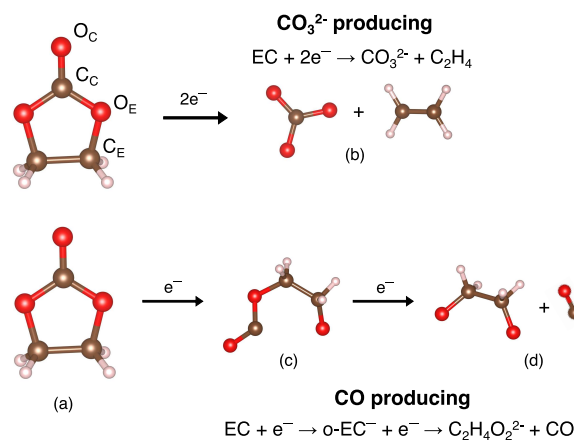


Figure 1. (a) Ethylene carbonate (EC) molecule decomposing via a two-electron route to produce (b) C_2H_4 and CO_3^{2-} or in two one-electron steps to produce an (c) o-EC[−] configuration followed by (d) CO and $\text{C}_2\text{H}_4\text{O}_2^{2-}$.

first is a fast two-electron reduction which cleaves both $\text{C}_E\text{--O}_E$ bonds (Figure 1a) to produce ethylene gas (C_2H_4) and a carbonate ion (CO_3^{2-}), as shown in Figure 1b. Alternatively, the two $\text{C}_C\text{--O}_E$ can break in sequence, first producing an o-EC[−] intermediate (Figure 1c), and then producing CO gas and a $\text{C}_2\text{H}_4\text{O}_2^{2-}$ ion (Figure 1d); however, the $\text{C}_2\text{H}_4\text{O}_2^{2-}$ ion is highly reactive, and likely goes on to produce other compounds such as CO, C_2H_4 , CO_3^{2-} , or ethylene dicarbonate.^{32,63,68,69} C_2H_4 and CO gas have both been detected experimentally in Li ion batteries as the result of EC decomposition.^{70–72}

3.1. Lithium, Pure EC. We first investigated the decomposition of 30 EC molecules on an (001) Li metal surface at 350 and 450 K. Although this system has been studied in the past, both computationally and experimentally, we did this to validate our AIMD method and compare our results with previous observations.^{60,61,64–66,73–76} In the case of pure EC, we did not find any molecules break to form CO_3^{2-} within 10 ps at either temperature, consistent with previous quantum chemical studies of EC reduction, although there are many other potential products.^{60,63,73} All rings that decomposed produced CO and $\text{C}_2\text{H}_4\text{O}_2^{2-}$, with the first one breaking at approximately 50 fs at both temperatures; the number of EC rings broken as a function of simulation time is shown in Figure 2a for 350 and 450 K. Interestingly, this is slightly different than EC reduction on Si anodes, where CO_3^{2-} ions form even in the absence of a LiPF_6 salt.^{77–79} The EC ring

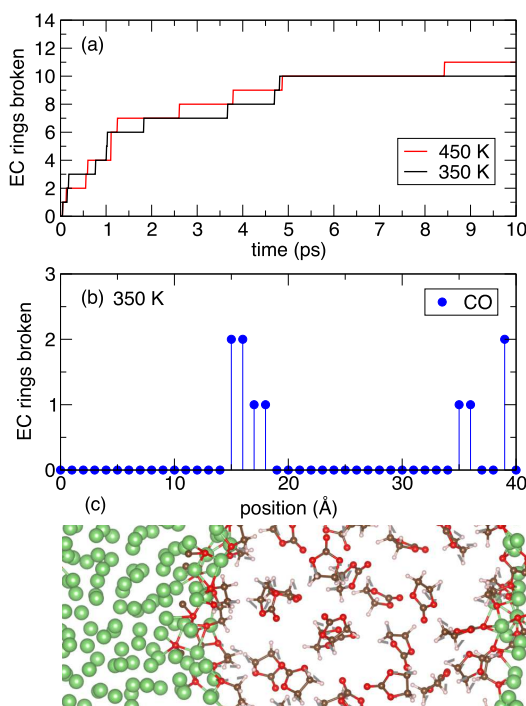


Figure 2. (a) Number of EC rings broken as a function of AIMD simulation time at 350 and 450 K in a system of 30 EC molecules on a Li metal surface. (b) Position at which EC rings break in the simulation cell at 350 K summed over the 10 ps trajectory. (c) EC decomposition on a Li metal surface after a 10 ps AIMD trajectory at 350 K.

opening then proceeds quickly, with 6 rings breaking after 1.5 ps at both temperatures. Following this, the rate of ring breaking slows, with one EC ring decomposing every 1–2 ps (with the rate being slightly faster at 450 K, as expected) and eventually saturates at 10 at 350 K and 11 at 450 K.

We next determined the position in the unit cell where each EC ring broke relative to the Li metal surface (Figure 2b for 350 K). There are two Li surfaces owing to the periodic boundary conditions used in DFT calculations (Figure 2c), resulting in the two observed regions of EC ring breaking. As expected, we found the EC molecules next to the surface are the ones which decompose; interestingly, however, some EC rings broke nearly 4 Å away from the Li surface. At 350 K, we found that the CO molecules intercalated approximately 4 to 5 Å into the Li metal while the $C_2H_4O_2^{2-}$ molecules remained on top of the surface in a layer that is 3 to 4 Å thick. The EC rings broke at very similar positions at 450 K (Supplemental Figure S1), but some CO molecules intercalated further than at 350 K; the $C_2H_4O_2^{2-}$ species again formed a thin layer on top of the metal. Finally, we investigated how each EC molecule was oriented relative to the Li surface when it broke. We quantified this by defining an angle between the EC molecule and the x , y , and z directions of the unit cell; a schematic showing this definition is shown in Supplemental Figure S2a. As shown in Supplemental Figure S2b, there is no correlation between the orientation of the EC molecule relative to any direction and when it breaks at both 350 and 450 K.

3.2. Lithium, EC/LiPF₆. We next replaced one of the EC molecules with a LiPF₆ molecule and ran a 10 ps AIMD trajectory at 350 and 450 K. The first notable difference between this system and pure EC is that we found a much faster rate of ring breaking; in this electrolyte, 8 EC rings had

broken at both temperatures by 2 ps (Figure 3a). Similar to the pure EC case, the number of rings broken saturated at 10 for

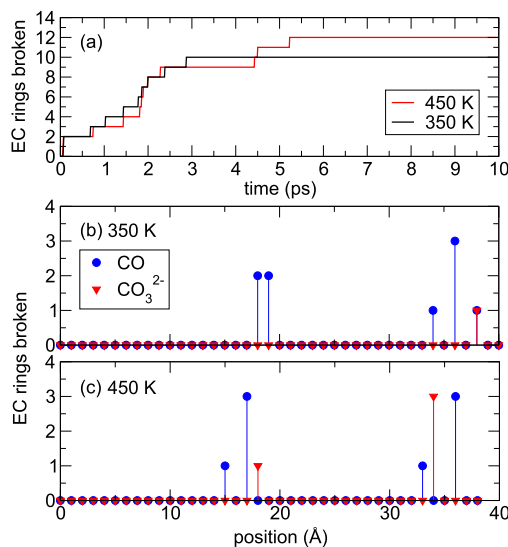


Figure 3. (a) Number of EC rings broken as a function of AIMD simulation time at 350 and 450 K in a system of 29 EC molecules and one LiPF₆ molecule on a Li metal surface. (b) Position at which EC rings break in the simulation cell at 350 K summed over the 10 ps trajectory. (c) Position at which EC rings break in the simulation cell at 450 K summed over the 10 ps trajectory.

350 K and 12 for 450 K. Furthermore, we found that 1 molecule of CO_3^{2-} was produced during the 350 K simulation, while 4 molecules of CO_3^{2-} were produced at 450 K. This is significantly more than in the other systems under study in this manuscript, as well as more than in previous studies of this system.^{61,64–66,74} This difference in the products of the decomposition of pure EC and EC/LiPF₆ is likely due to the lowering of the EC concentration by introducing the LiPF₆ salt. Previous work on EC reduction in Li-based systems has indeed demonstrated that lower concentrations of EC preferentially form CO_3^{2-} .^{60,73} This is also consistent with our previous studies on Ca metal surfaces showing that an isolated EC molecule decomposes to form a carbonate ion, while having two or more molecules on the surface (i.e., more packed) results only in $C_2H_4O_2^{2-}$.²⁰

Similar to the pure EC case, we found that the position at which the rings break extends a small distance away from the metal surface, with no specific favored position for the production of CO or CO_3^{2-} (Figure 3b and c for 350 and 450 K, respectively). Furthermore, the orientation of the molecule again has no determination on when it breaks. While it is likely that the $C_2H_4O_2^{2-}$ would further decompose or react to form other organic components, as it is a highly reactive species as described previously,^{32,63,68,69} we find that the CO_3^{2-} species react with Li to form Li_2CO_3 . Furthermore, the PF₆⁻ anion begins to decompose after about 1 to 2 ps, after which the F atoms go on to form LiF. Both Li_2CO_3 and LiF are known to be major inorganic components of the SEL.²⁴ Finally, the Li⁺ ion from the salt eventually becomes coordinated by 4 EC molecules to form the first solvation shell, consistent with previous experimental and computational studies.^{80–83} Representative snapshots of the AIMD simulations with these species indicated are shown in Supplemental Figure S4a and b for the systems at 350 and 450 K, respectively.

3.3. Calcium, EC/Ca(PF₆)₂. We next investigated the decomposition of EC and a Ca(PF₆)₂ salt on an (001) Ca surface, a salt which was recently reported to be synthesized and used in a Ca ion battery with a tin anode.^{37,84} At both 350 and 450 K, we found that only CO and C₂H₄O₂²⁻ molecules were produced by the breakdown of EC in this electrolyte, in contrast to the EC/LiPF₆ case described in the previous section. Furthermore, the decomposition of EC proceeds much faster than in the case of a Li metal surface, with 6 to 7 EC rings broken within 1 ps at 350 and 450 K (Figure 4a). The

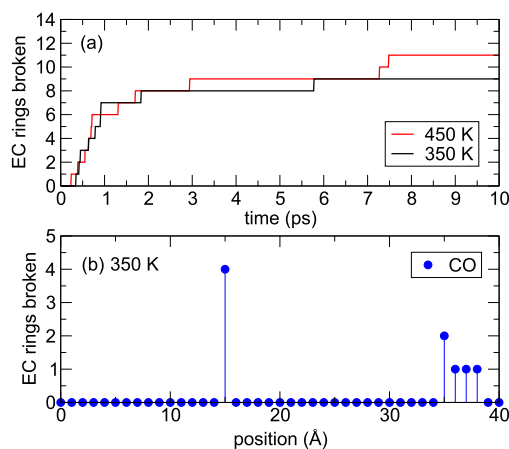


Figure 4. (a) Number of EC rings broken as a function of AIMD simulation time at 350 and 450 K in a system of 29 EC molecules and one Ca(PF₆)₂ molecule on a Ca metal surface. (b) Position at which EC rings break in the simulation cell at 350 K summed over the 10 ps trajectory.

ring breaking saturates after this, however, with only 2 additional EC rings breaking within 10 ps at 350 K (for a total of 9), and 4 additional EC rings breaking within 10 ps at 450 K (for a total of 11). The EC rings near the Ca surface are again the ones that break, with one of the layers extending nearly 4 Å (Figure 4b at 350 K). This is similar at 450 K (Supplemental Figure S5). Furthermore, the size of the first solvation shell increases compared to the Li case, with 5 EC coordinating the Ca²⁺ ion, similar to what was found in the case of Ca(ClO₄)₂ in our previous work.²⁰ This is in agreement with the solvation structure predicted for Mg²⁺ cations in pure EC;⁸⁵ however, the solvation of Ca in EC has not been significantly studied, but this larger shell likely impacts the Ca ion mobility through the electrolyte. As in the Li metal case, there is no dependence on the orientation of the EC molecules on the surface and when they decompose (Supplemental Figure S6).

As in the Li case and our previous study of Ca systems,²⁰ CO molecules intercalated into the metal surface; however, they only intercalated to a maximum of 2.5 Å into the surface, much less than in the Li system. The C₂H₄O₂²⁻ species remained on the surface in a layer approximately 4 Å thick. We constructed this system to have one PF₆⁻ ion near the Ca surface and one in the middle of the unit cell. Interestingly, the PF₆⁻ ion near the surface decomposed while the ion in the middle of the electrolyte remained completely intact after 10 ps. At 350 K, the PF₆⁻ ion began to quickly decompose at approximately 2.1 ps, with 3 F atoms released by 2.3 ps. After this, however, the new PF₃ remained relatively stable, only completely decomposing at 3.6 ps. Similarly, 3 F atoms were

released from the PF₆⁻ ion near the Ca surface at 450 K over the course of 1.6 to 1.9 ps, slightly faster than at 350 K. However, the PF₃ species produced remained intact for much longer than at 350 K, only fully decomposing at 6.3 ps. At both 350 and 450 K the F atoms bonded to Ca atoms at the surface, forming a CaF₂ network; this is in agreement with compounds found on the tin anode in a Ca ion battery using an EC:PC/Ca(PF₆)₂ electrolyte.³⁷ Representative snapshots at 10 ps at both 350 and 450 K are shown in Supplemental Figure S7a and b, respectively.

3.4. Aluminum, Pure EC. Finally, we investigated the breakdown of pure EC and an EC/AlCl₃ electrolyte on an (001) Al surface. In the case of pure EC, no CO₃²⁻ ions were produced in either of the simulations at 350 or 450 K, similar to the case of Li and our previous work on bulk Ca.²⁰ The rate of EC ring breaking is much slower on the Al metal surface than either Li or Ca, with only 4 EC rings breaking by 1 ps for both 350 and 450 K (Figure 5a). This rate slows even further,

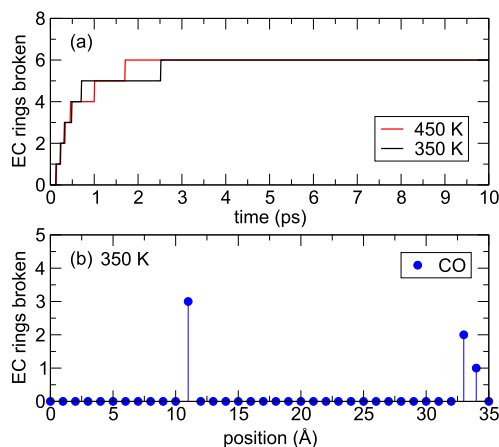


Figure 5. (a) Number of EC rings broken as a function of AIMD simulation time at 350 and 450 K in a system of 30 EC molecules on an Al metal surface. (b) Position at which EC rings break in the simulation cell at 350 K summed over the 10 ps trajectory.

and the number of EC rings broken by 10 ps saturates at only 6 at both temperatures. The thickness of the layer of C₂H₄O₂²⁻ on the Al surface is therefore smaller than that of pure EC on Li or Ca (only about 2 Å, Figure 5b for 350 K and Supplemental Figure S8 for 450 K). Interestingly, unlike the Li or Ca case, no CO molecules intercalate into the Al metal, instead sitting on the surface with the C₂H₄O₂²⁻ ions; this results in much less amorphization of the Al metal surface, likely due to the increased strength of the metallic bonding in Al compared to Ca and Li. Finally, like the Li and Ca case, the orientation of the molecule relative to the Al surface has no bearing on its decomposition.

3.5. Aluminum, EC/AlCl₃. As with pure EC on Al, when one of the EC molecules is replaced by a molecule of AlCl₃ the rate of EC ring breaking is still much slower than the Li or Ca case; after 1 ps only 2 and 4 EC molecules decompose at 350 and 450 K, respectively (Figure 6a). However, we do now find that one EC ring at each temperature breaks to form CO₃²⁻ and C₂H₄. At both 350 and 450 K, the EC ring initially breaks relatively far from the surface (approximately 4 to 5 Å away, Figure 6b for 350, Supplemental Figure S9 for 450 K). The CO₃²⁻ species then moves to sit next to the surface but neither intercalates nor binds with any of the Al atoms. Additionally, as

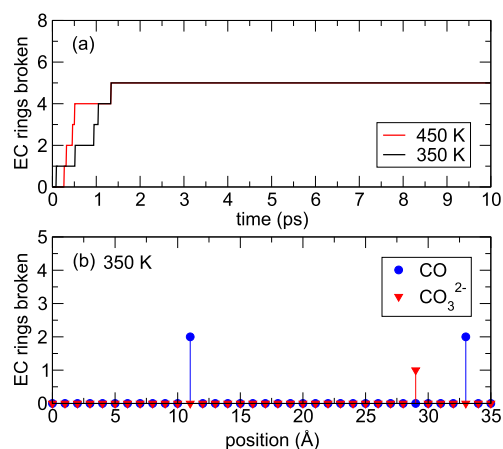


Figure 6. (a) Number of EC rings broken as a function of AIMD simulation time at 350 and 450 K in a system of 29 EC molecules and one AlCl₃ molecule on an Al metal surface. (b) Position at which EC rings break in the simulation cell at 350 K summed over the 10 ps trajectory.

with pure EC, the CO molecules do not intercalate into the metal surface but instead sit on top with the C₂H₄O₂²⁻ species. Finally, the AlCl₃ salt does not break down at either 350 or 450 K.

We next replaced two EC molecules with two AlCl₃ salt molecules and ran a 10 ps trajectory at 350 and 450 K. At 350 K we find that 4 EC rings break to form CO and C₂H₄O₂²⁻ within 0.5 ps, with one more ring breaking at 1 ps; no additional rings decompose up to 10 ps (black line, Figure 7a).

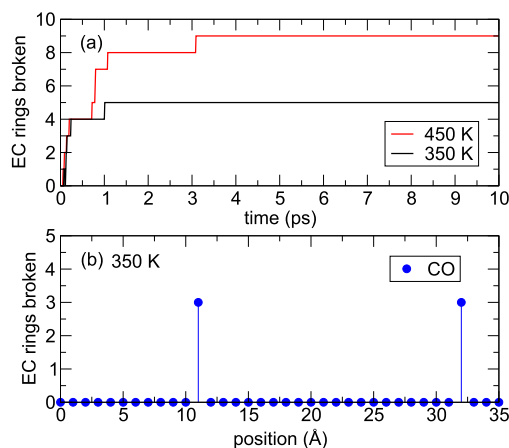


Figure 7. (a) Number of EC rings broken as a function of AIMD simulation time at 350 and 450 K in a system of 28 EC molecules and two AlCl₃ molecules on an Al metal surface. (b) Position at which EC rings break in the simulation cell at 350 K summed over the 10 ps trajectory.

The CO and C₂H₄O₂²⁻ molecules again sit on the Al metal surface and form a thin layer (this can be seen schematically in Figure 7b). As before, neither of the AlCl₃ salt molecules decompose. However, at 450 K we find significantly different behavior. First, the rate of ring breaking is much faster than any of the other Al surface simulations, with 8 EC rings breaking within 1 ps, and saturating at 10 broken rings (red line, Figure 7a); however, the EC rings broke only to form CO and C₂H₄O₂²⁻. This significantly increases the thickness of the SEI layer compared to the other Al metal surface simulations, as

seen by where in the simulation cell the EC molecules broke (Supplemental Figure S10). Furthermore, one Cl ion transfers from one of the AlCl₃ molecules to the other, resulting in formation of an AlCl₄⁻ species (Supplemental Figure S11); this molecule is well-known to form in Al batteries utilizing AlCl₃ salt.⁸⁶ However, no other inorganic or organic compounds were formed.

To determine the origin of the differences in the rate of electrolyte breakdown on the multivalent surfaces, we next investigated the charge transfer on Ca and Al metal. To do this, we computed the Bader charge density every 100 fs for the first 2 ps of the Ca and Al AIMD simulations. These results are summarized in Figure 8, where we have plotted the number of

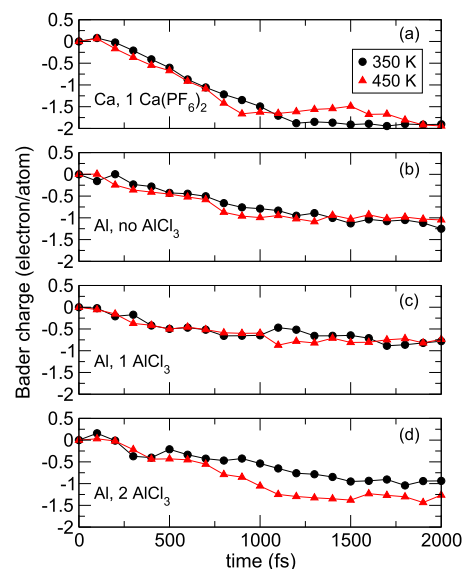


Figure 8. Charge transferred from the top layer of the metal surface to the electrolyte (normalized to the number of atoms) in a system consisting of (a) Ca metal and a 29 EC/1 Ca(PF₆)₂ molecule electrolyte, (b) Al metal and a 30 EC molecule electrolyte, (c) Al metal and a 29 EC/1 AlCl₃ molecule electrolyte, and (d) Al metal and a 28 EC/2 AlCl₃ molecule electrolyte at 350 and 450 K (black circles and red triangles, respectively).

charge transferred from the metal to the electrolyte from the top layer of the surface, normalized to the number of atoms making up the surface; this was done at both 350 K (black circles) and 450 K (red triangles). In the case of Ca (Figure 8a), we find that the charge transferred from the surface steadily increases until 2 electrons are transferred per atom. This saturation occurs slightly sooner at 450 K (900 fs) than at 350 K (1200 fs) and is expected given the divalent nature of the Ca atoms. Interestingly, however, only one electron per Al atom is transferred over the same simulation time period. This is the same whether there are zero AlCl₃ (Figure 8b), one AlCl₃ (Figure 8c), or two AlCl₃ (Figure 8d). The only deviation occurs in the two AlCl₃ system at 450 K, where 1.5 electrons are transferred from every Al atom; this increase in the charge transfer is responsible for the observed faster EC breaking rate described previously. The difference between the Ca and Al case is likely due to differences in the ionization energy and electronegativity of these two species (all numbers obtained from ref 87). The ionization energy for the first two electrons of Ca are 6.11 and 11.9 eV; although the first ionization energy of Al is similar at 5.98 eV, the second (18.8

eV) and third (28.4 eV) are higher. Moreover, the electronegativity of Ca (1.00) is lower than Al (1.61). Thus, it is significantly easier for Ca to transfer charge to the electrolyte than Al. A similar case can be made for Li, which has a first ionization energy of 5.39 eV and an electronegativity close to Ca (0.98); indeed, a Bader charge analysis has been performed previously for EC on Li metal and found charge transfer to act similarly.⁶¹ This therefore gives rise to the observed differences in electrolyte breakdown rate in these systems.

Finally, we note several differences between simulations with and without salt molecules; to make this comparison easier, we have replotted the data showing the number of EC rings broken as a function of simulation time with and without a salt molecule at a given temperature (Supplemental Figures S12, S13, and S14). We have also included our data from a previous study to draw comparisons between those Ca-based systems as well.²⁰ On the Li metal surface, we find that the rate of EC ring breaking is slightly faster in the system with no salt than the one with an LiPF₆ molecule up to 2 ps at both 350 and 450 K (Supplemental Figure S12a and b, respectively). After this, the EC rings break faster in the simulation containing a salt than without until saturation at 10–12 EC rings broken. On the Ca metal surface, we find that the presence of a Ca(ClO₄)₂ salt results in the slowest rate of EC ring breaking at both 350 and 450 K (Supplemental Figure S13a and b). The simulations containing no salt and a Ca(PF₆)₂ molecule exhibit a similar rate at both temperatures. At 350 K, however, after 2 ps the pure EC rate increases compared to either of those containing a salt molecule. Furthermore, at 450 K, the decomposition rates are similar after 3 ps for all three systems. Finally, the salt concentration seems to make no difference on the Al metal surface at 350 K (Supplemental Figure S14a). However, at 450 K, decomposition rate in the simulation containing 2 AlCl₃ salt molecules far outpaces the other two simulations, in which the EC rings break at a similar rate (Supplemental Figure S14b); as described previously, this is due to the increased charge transfer into this system from the Al metal surface (Figure 8d). Increasing the AlCl₃ concentration likely increases the probability of AlCl₄⁻ formation (which occurred here in the system at 450 K), in turn facilitating additional charge transfer from the Al surface. In every other case discussed here (i.e., besides the Al system with 2 AlCl₃ salt molecules at 450 K), the addition of a salt slightly slows the initial stages of EC ring breaking rate; however, the number of broken EC rings in simulations on the same metal surface and at the same temperature eventually saturate at close to the same value after 10 ps. These differences yield some insight into how salt concentration can affect the initial stages of SEI formation; the addition of a salt molecule appears to slightly slow the electrolyte decomposition rate, at least at the very initial stages. Indeed, the concentration of the salt, in addition to its chemical makeup, can play an important role in determining the properties and formation of the SEI and the ionic transport properties of the electrolyte;^{24,37,88–93} this provides another parameter to tune in the design of electrolytes²¹ and deserves further study, especially in emerging multivalent ion technology.

4. CONCLUSION

In this work, we performed a comparative study of the initial stages of pure EC and EC-based electrolytes on Li, Ca, and Al metal anodes. We found that while EC decomposition is fast on Li and Ca metal surfaces, it is slower on Al metal. By

computing the Bader charges, we showed that this is because the amount of charge transferred is larger and occurs faster in Ca than Al. Furthermore, we found that the EC rings break only along the route that produces CO and C₂H₄O₂²⁻ molecules; EC only forms CO₃²⁻ and C₂H₄ when a salt molecule is present. Finally, we found that the inorganic compounds that form depend on the salt in the electrolyte. Using AIMD calculations, we have shown that the products formed here on short time scales closely match those observed experimentally. Besides being able to study the effect of electrolyte composition on the SEI, this molecular level understanding of decomposition and SEI formation can be extended to computationally investigate new electrolytes and predict the composition of the SEI before synthesis. We hope that these results inspire the investigation of tailored electrolytes for beyond-Li ion batteries.

■ ASSOCIATED CONTENT

Supporting Information

The Supporting Information is available free of charge on the ACS Publications website at DOI: 10.1021/acsam.8b01707.

Position plots of EC ring breaking at 450 K EC orientation relative to metal surface upon breaking, additional AIMD snapshots, EC rings broken as a function of simulation time (PDF)

■ AUTHOR INFORMATION

Corresponding Authors

*E-mail: jayoung@binghamton.edu.

*E-mail: msmeu@binghamton.edu.

ORCID

Joshua Young: 0000-0001-8102-751X

Manuel Smeu: 0000-0001-9548-4623

Notes

The authors declare no competing financial interest.

■ ACKNOWLEDGMENTS

J.Y. and M.S. were supported by funding from Binghamton University. P.K. was supported by the National Science Foundation Research Experiences for Undergraduates Program (DMR-1658990) and Binghamton University's Transdisciplinary Area of Excellence in Smart Energy. T.J. was supported as part of the Multidisciplinary GAANN in Smart Energy Materials, a Graduate Areas of National Need, funded by the U.S. Department of Education, under Award P200A150135. DFT calculations were performed on the Spiedie cluster at Binghamton University, the Extreme Science and Engineering Discovery Environment (XSEDE, supported by NSF Grant No. ACI-1053575) under allocation TG-DMR180009, and the CARBON cluster at the Center for Nanoscale Materials (Argonne National Laboratory, supported by the U.S. DOE, Office of Basic Energy Sciences (BES), DE-AC02-06CH11357) under allocation CNMS9122.

■ REFERENCES

- (1) Tester, J. W.; Drake, E. M.; Driscoll, M. J.; Golay, M. W.; Peters, W. A. *Sustainable Energy: Choosing Among Options*; The MIT Press, 2012.
- (2) Dunn, B.; Kamath, H.; Tarascon, J.-M. Electrical Energy Storage for the Grid: A Battery of Choices. *Science* **2011**, *334*, 928–935.

- (3) Gür, T. M. Review of electrical energy storage technologies, materials and systems: challenges and prospects for large scale grid storage. *Energy Environ. Sci.* **2018**, *11*, 2696.
- (4) Nitta, N.; Wu, F.; Lee, J. T.; Yushin, G. Li-ion battery materials: present and future. *Mater. Today* **2015**, *18*, 252.
- (5) Tarascon, J.-M.; Armand, M. Issues and challenges facing rechargeable lithium batteries. *Nature* **2001**, *414*, 359–367.
- (6) van Noorden, R. A Better Battery. *Nature* **2014**, *507*, 26.
- (7) Everts, E. C. Lithium batteries: To the limits of lithium. *Nature* **2015**, *526*, S93–S95.
- (8) Choi, J. W.; Aurbach, D. Promise and reality of post-lithium-ion batteries with high energy densities. *Nature Rev. Mater.* **2016**, *1*, 16013.
- (9) Bruce, P. G.; Freunberger, S. A.; Hardwick, L. J.; Tarascon, J.-M. Li₂O₂ and Li₂S batteries with high energy storage. *Nat. Mater.* **2012**, *11*, 19–29.
- (10) Lin, D.; Liu, Y.; Cui, Y. Reviving the lithium metal anode for high-energy batteries. *Nat. Nanotechnol.* **2017**, *12*, 194–206.
- (11) Eroglu, D.; Ha, S.; Gallagher, K. G. Fraction of the Theoretical Specific Energy Achieved on Pack Level for Hypothetical Battery Chemistries. *J. Power Sources* **2014**, *267*, 14–19.
- (12) Muldoon, J.; Bucur, C. B.; Gregory, T. Quest for Nonaqueous Multivalent Secondary Batteries: Magnesium and Beyond. *Chem. Rev.* **2014**, *114*, 11683–11720.
- (13) Yoo, H. D.; Shterenberg, I.; Gofer, Y.; Gershinshy, G.; Pour, N.; Aurbach, D. Mg rechargeable batteries: an on-going challenge. *Energy Environ. Sci.* **2013**, *6*, 2265.
- (14) Elia, G. A.; Marquardt, K.; Fantini, S.; Lin, R.; Knipping, E.; Peters, W.; Drillet, J. F.; Passerini, S.; Hahn, R.; Hoepfner, K. An Overview and Future Perspectives of Aluminum Batteries. *Adv. Mater.* **2016**, *28*, 7564–7579.
- (15) Dompablo, M. E.; Krich, C.; Nava-Avendaño, J.; Biskup, N.; Palacin, M. R.; Bardé, F. A Joint Computational and Experimental Evaluation of CaMn₂O₄ Polymorphs as Cathode Materials for Ca Ion Batteries. *Chem. Mater.* **2016**, *28*, 6886–6893.
- (16) Tojo, T.; Sugiura, Y.; Inada, R.; Sakurai, Y. Reversible Calcium Ion Batteries Using a Dehydrated Prussian Blue Analogue Cathode. *Electrochim. Acta* **2016**, *207*, 22–27.
- (17) Juran, T. R.; Smeu, M. Hybrid Density Functional Theory Modeling of Ca, Zn, and Al Ion Batteries Using the Chevrel Phase Mo₆S₈ Cathode. *Phys. Chem. Chem. Phys.* **2017**, *19*, 20684–20690.
- (18) Smeu, M.; Hossain, M. S.; Wang, Z.; Timoshevskii, V.; Bevan, K. H.; Zaghbi, K. Theoretical Investigation of Chevrel Phase Materials for Cathodes Accommodating Ca²⁺ Ions. *J. Power Sources* **2016**, *306*, 431–436.
- (19) Juran, T.; Young, J.; Smeu, M. Density Functional Theory Modeling of MnO₂ Polymorphs as Cathodes for Multivalent Ion Batteries. *J. Phys. Chem. C* **2018**, *122*, 8788–8795.
- (20) Young, J.; Smeu, M. Ethylene Carbonate-Based Electrolyte Decomposition and Solid Electrolyte Interphase Formation on Ca Metal Anodes. *J. Phys. Chem. Lett.* **2018**, *9*, 3295–3300.
- (21) Qu, X.; Jain, A.; Rajput, N. N.; Cheng, L.; Zhang, Y.; Ong, S. P.; Brafman, M.; Maginn, E.; Curtiss, L. A.; Persson, K. A. The Electrolyte Genome project: A big data approach in battery materials discovery. *Comput. Mater. Sci.* **2015**, *103*, 56–67.
- (22) Gummow, R. J.; Vamvounis, G.; Kannan, M. B.; He, Y. Calcium-Ion Batteries: Current State-of-the-Art and Future Perspectives. *Adv. Mater.* **2018**, *30*, 1801702.
- (23) Ponrouch, A.; Palacin, M. R. On the road toward calcium-based batteries. *Curr. Opin. Electrochem.* **2018**, *9*, 1–7.
- (24) Xu, K. Electrolytes and Interphases in Li-Ion Batteries and Beyond. *Chem. Rev.* **2014**, *114*, 11503–11618.
- (25) Goodenough, J. B.; Kim, Y. Challenges for rechargeable Li batteries. *Chem. Mater.* **2010**, *22*, 587–603.
- (26) Peled, E. The Electrochemical Behavior of Alkali and Alkaline Earth Metals in Non-aqueous Battery Systems—The Solid Electrolyte Interphase Model. *J. Electrochem. Soc.* **1979**, *126*, 2047–2051.
- (27) Aurbach, D.; Daroux, M. L.; Faguy, P. W.; Yeager, E. Identification of Surface Films Formed on Lithium in Propylene Carbonate Solutions. *J. Electrochem. Soc.* **1987**, *134*, 1611–1620.
- (28) Aurbach, D.; Ein-Ely, Y.; Zaban, A. The Surface Chemistry of Lithium Electrodes in Alkyl Carbonate Solutions. *J. Electrochem. Soc.* **1994**, *141*, L1–L3.
- (29) Peled, E.; Golodnitsky, D.; Ardel, G. Advanced Model for Solid Electrolyte Interphase Electrodes in Liquid and Polymer Electrolytes. *J. Electrochem. Soc.* **1997**, *144*, L208–L210.
- (30) Verma, P.; Maire, P.; Novák, P. A review of the features and analyses of the solid electrolyte interphase in Li-ion batteries. *Electrochim. Acta* **2010**, *55*, 6332–6341.
- (31) An, S. J.; Li, J.; Daniel, C.; Mohanty, D.; Nagpure, S.; Wood, D. L. The state of understanding of the lithium-ion-battery graphite solid electrolyte interphase (SEI) and its relationship to formation cycling. *Carbon* **2016**, *105*, 52–76.
- (32) Peled, E.; Menkin, S. SEI: Past, Present and Future. *J. Electrochem. Soc.* **2017**, *164*, A1703–A1719.
- (33) Cheng, X.-B.; Zhang, R.; Zhao, C.-Z.; Wei, F.; Zhang, J.-G.; Zhang, Q. A Review of Solid Electrolyte Interphases on Lithium Metal Anode. *Adv. Sci.* **2016**, *3*, 1500213.
- (34) Aurbach, D.; Skaletsky, R.; Gofer, Y. The Electrochemical Behavior of Calcium Electrodes in a Few Organic Electrolytes. *J. Electrochem. Soc.* **1991**, *138*, 3536.
- (35) Tchitchekova, D. S.; Monti, D.; Johansson, P.; Bardé, F.; Randon-Vitanova, R.; Palacin, M. R.; Ponrouch, A. On the Reliability of Half-Cell Tests for Monovalent (Li⁺, Na⁺) and Divalent (Mg²⁺, Ca²⁺) Cation Based Batteries. *J. Electrochem. Soc.* **2017**, *164*, A1384–A1392.
- (36) Ponrouch, A.; Frontera, C.; Bardé, F.; Palacin, M. R. Towards a calcium-based rechargeable battery. *Nat. Mater.* **2016**, *15*, 169–172.
- (37) Wang, D.; Gao, X.; Chen, Y.; Jin, L.; Kuss, C.; Bruce, P. G. Plating and stripping calcium in an organic electrolyte. *Nat. Mater.* **2017**, *17*, 16–20.
- (38) Markovsky, B.; Amalraj, F.; Gottlieb, H. E.; Gofer, Y.; Marth, S. K.; Aurbach, D. On the Electrochemical Behavior of Aluminum Electrodes in Nonaqueous Electrolyte Solutions of Lithium Salts. *J. Electrochem. Soc.* **2010**, *157*, A423–A429.
- (39) Licht, S.; Levitin, G.; Yarnitzky, C.; Tel-Vered, R. The Organic Phase for Aluminum Batteries. *Electrochem. Solid State Lett.* **2018**, *9*, 1–7.
- (40) Zhao, Y.; Vandernoot, T. J. Electrodeposition of aluminium from nonaqueous organic electrolytic systems and room temperature molten salts. *Electrochim. Acta* **1997**, *42*, 3–13.
- (41) Bai, L.; Conway, B. E. Complex Behavior of Al Dissolution in Non-Aqueous Medium as Revealed by Impedance Spectroscopy. *J. Electrochem. Soc.* **1990**, *137*, 3737–3747.
- (42) Das, S. K.; Mahapatra, S.; Lahan, H. Aluminium-ion batteries: developments and challenges. *J. Mater. Chem. A* **2017**, *5*, 6347–6367.
- (43) Reed, L. D.; Ortiz, S. N.; Xiong, M.; Menke, E. J. A rechargeable aluminum-ion battery utilizing a copper hexacyanoferrate cathode in an organic electrolyte. *Chem. Commun.* **2015**, *51*, 14397–14400.
- (44) Jayaprakash, N.; Das, S. K.; Archer, L. A. The rechargeable aluminum-ion battery. *Chem. Commun.* **2011**, *47*, 12610–12612.
- (45) Xing, L.; Zheng, X.; Schroeder, M.; Alvarado, J.; von Wald Cresce, A.; Xu, K.; Li, Q.; Li, W. Deciphering the Ethylene Carbonate-Propylene Carbonate Mystery in Li-Ion Batteries. *Acc. Chem. Res.* **2018**, *51*, 282–289.
- (46) Tikekar, M. D.; Choudhury, S.; Tu, Z.; Archer, L. A. Design principles for electrolytes and interfaces for stable lithium-metal batteries. *Nature Energy* **2016**, *1*, 16114.
- (47) Car, R.; Parrinello, M. Unified Approach for Molecular Dynamics and Density-Functional Theory. *Phys. Rev. Lett.* **1985**, *55*, 2471.
- (48) Hohenberg, P.; Kohn, W. Inhomogeneous Electron Gas. *Phys. Rev.* **1964**, *136*, B864–B871.
- (49) Kohn, W.; Sham, J. L. Self-Consistent Equations Including Exchange and Correlation Effects. *Phys. Rev.* **1965**, *140*, A1133.

- (50) Kresse, G.; Hafner, J. *Ab initio* molecular dynamics for liquid metals. *Phys. Rev. B: Condens. Matter Mater. Phys.* **1993**, *47*, 558–561.
- (51) Kresse, G.; Furthmüller, J. Efficiency of *ab-initio* total energy calculations for metals and semiconductors using a plane-wave basis set. *Comput. Mater. Sci.* **1996**, *6*, 15–30.
- (52) Kresse, G.; Furthmüller, J. Efficient iterative schemes for *ab initio* total-energy calculations using a plane-wave basis set. *Phys. Rev. B: Condens. Matter Mater. Phys.* **1996**, *54*, 11169.
- (53) Blöchl, P. E. Projector augmented-wave method. *Phys. Rev. B: Condens. Matter Mater. Phys.* **1994**, *50*, 17953–17979.
- (54) Perdew, J. P.; Ruzsinszky, A.; Csonka, G. I.; Vydrov, O. A.; Scuseria, G. E.; Constantin, L. A.; Zhou, X.; Burke, K. Restoring the Density-Gradient Expansion for Exchange in Solids and Surfaces. *Phys. Rev. Lett.* **2008**, *100*, 136406.
- (55) Martinez, L.; Andrade, R.; Birgin, E. G.; Martinez, J. M. Packmol: A package for building initial configurations for molecular dynamics simulations. *J. Comput. Chem.* **2009**, *30*, 2157–2164.
- (56) Henkelman, G.; Arnaldsson, A.; Jónsson, H. A fast and robust algorithm for Bader decomposition of charge density. *Comput. Mater. Sci.* **2006**, *36*, 354–360.
- (57) Sanville, E.; Kenny, S. D.; Smith, R.; Henkelman, G. Improved Grid-Based Algorithm for Bader Charge Allocation. *J. Comput. Chem.* **2007**, *28*, 899–908.
- (58) Tang, W.; Sanville, E.; Henkelman, G. A grid-based Bader analysis algorithm without lattice bias. *J. Phys.: Condens. Matter* **2009**, *21*, No. 084204.
- (59) Yu, M.; Trinkle, D. R. Accurate and efficient algorithm for Bader charge integration. *J. Chem. Phys.* **2011**, *134*, No. 064111.
- (60) Wang, Y.; Nakamura, S.; Ue, M.; Balbuena, P. B. Theoretical Studies To Understand Surface Chemistry on Carbon Anodes for Lithium-Ion Batteries: Reduction Mechanisms of Ethylene Carbonate. *J. Am. Chem. Soc.* **2001**, *123*, 11708–11718.
- (61) Ebadi, M.; Brandell, D.; Araujo, C. M. Electrolyte decomposition on Li-metal surfaces from first-principles theory. *J. Chem. Phys.* **2016**, *145*, 204701.
- (62) Yu, J.; Balbuena, P. B.; Budzien, J.; Leung, K. Hybrid DFT Functional-Based Static and Molecular Dynamics Studies of Excess Electron in Liquid Ethylene Carbonate. *J. Electrochem. Soc.* **2011**, *158*, A400–A410.
- (63) Leung, K. Two-electron reduction of ethylene carbonate: A quantum chemistry re-examination of mechanisms. *Chem. Phys. Lett.* **2013**, *568–569*, 1–8.
- (64) Islam, M. M.; van Duin, A. C. T. Reductive Decomposition Reactions of Ethylene Carbonate by Explicit Electron Transfer from Lithium: An eReaxFF Molecular Dynamics Study. *J. Phys. Chem. C* **2016**, *120*, 27128–27134.
- (65) Ganesh, P.; Kent, P. R. C.; Jiang, D.-E. Solid-Electrolyte Interphase Formation and Electrolyte Reduction at Li-Ion Battery Graphite Anodes: Insights from First-Principles Molecular Dynamics. *J. Phys. Chem. C* **2012**, *116*, 24476–24481.
- (66) Brennan, M. D.; Breedon, M.; Best, A. S.; Morishita, T.; Spencer, M. J. S. Surface Reactions of Ethylene Carbonate and Propylene Carbonate on the Li(001) Surface. *Electrochim. Acta* **2017**, *243*, 320–330.
- (67) Leung, K.; Budzien, J. *Ab initio* molecular dynamics simulations of the initial stages of solid?electrolyte interphase formation on lithium ion battery graphitic anodes. *Phys. Chem. Chem. Phys.* **2010**, *12*, 6583–6586.
- (68) Lee, J.-C.; Litt, M. H. Ring-Opening Polymerization of Ethylene Carbonate and Depolymerization of Poly(ethylene oxide-co-ethylene carbonate). *Macromolecules* **2000**, *33*, 1618–1627.
- (69) Zhuang, G. V.; Xu, K.; Yang, H.; Jow, T. R.; Ross, P. N. Lithium Ethylene Dicarboxylate Identified as the Primary Product of Chemical and Electrochemical Reduction of EC in 1.2 M LiPF₆/EC:EMC Electrolyte. *J. Phys. Chem. B* **2005**, *109*, 17567–17573.
- (70) Yoshida, H.; Fukunaga, T.; Hazama, T.; Terasaki, M.; Mizutani, M.; Yamachi, M. Degradation mechanism of alkyl carbonate solvents used in lithium-ion cells during initial charging. *J. Power Sources* **1997**, *68*, 311–315.
- (71) Ogumi, Z.; Sano, A.; Inaba, M.; Abe, T. Pyrolysis/gas chromatography/mass spectroscopy analysis of the surface film formed on graphite negative electrode. *J. Power Sources* **2001**, *97*, 156–158.
- (72) Onuki, M.; Kinoshita, S.; Sakata, Y.; Yanagidate, M.; Otake, Y.; Ue, M.; Deguchi, M. Identification of the Source of Evolved Gas in Li-Ion Batteries Using #2#1-Labeled Solvents. *J. Electrochem. Soc.* **2008**, *155*, A794.
- (73) Li, T.; Balbuena, P. B. Theoretical studies of the reduction of ethylene carbonate. *Chem. Phys. Lett.* **2000**, *317*, 421–429.
- (74) Leung, K.; Qi, Y.; Zavadil, K. R.; Jung, Y. S.; Dillon, A. C.; Cavanagh, A. S.; Lee, S.-H.; George, S. M. Using Atomic Layer Deposition to Hinder Solvent Decomposition in Lithium Ion Batteries: First-Principles Modeling and Experimental Studies. *J. Am. Chem. Soc.* **2011**, *133*, 14741–14754.
- (75) Leung, K. Electronic Structure Modeling of Electrochemical Reactions at Electrode/Electrolyte Interfaces in Lithium Ion Batteries. *J. Phys. Chem. C* **2013**, *117*, 1539–1547.
- (76) Gachot, G.; Grugeon, S.; Armand, M.; Pilard, S.; Guenot, P.; Tarascon, S.; Laruelle, J.-M. Deciphering the multi-step degradation mechanisms of carbonate-based electrolyte in Li batteries. *J. Power Sources* **2008**, *178*, 409–421.
- (77) Martinez de la Hoz, J. M.; Leung, K.; Balbuena, P. B. Reduction Mechanisms of Ethylene Carbonate on Si Anodes of Lithium-Ion Batteries: Effects of Degree of Lithiation and Nature of Exposed Surface. *ACS Appl. Mater. Interfaces* **2013**, *5*, 13457–13465.
- (78) Martinez de la Hoz, J. M.; Balbuena, P. B. Reduction mechanisms of additives on Si anodes of Li-ion batteries. *Phys. Chem. Chem. Phys.* **2014**, *16*, 17091–17098.
- (79) Martinez de la Hoz, J. M.; Soto, F. A.; Balbuena, P. B. Effect of the Electrolyte Composition on SEI Reactions at Si Anodes of Li-Ion Batteries. *J. Phys. Chem. C* **2015**, *119*, 7060–7068.
- (80) Hyodo, S.-A.; Okabayashi, K. Raman intensity study of local structure in non-aqueous electrolyte solutions?I. Cation-solvent interaction in LiClO₄/ethylene carbonate. *Electrochim. Acta* **1989**, *34*, 1551–1556.
- (81) von Wald Cresce, A.; Borodin, O.; Xu, K. Correlating Li⁺ Solvation Sheath Structure with Interphasial Chemistry on Graphite. *J. Phys. Chem. C* **2012**, *116*, 26111–26117.
- (82) Cui, W.; Lansac, Y.; Lee, H.; Hong, S.-T.; Jang, Y. H. Lithium ion solvation by ethylene carbonates in lithium-ion battery electrolytes, revisited by density functional theory with the hybrid solvation model and free energy correction in solution. *Phys. Chem. Chem. Phys.* **2016**, *18*, 23607–23612.
- (83) Borodin, O.; Ren, X.; Vatamanu, J.; von Wald Cresce, A.; Knap, J.; Xu, K. Modeling Insight into Battery Electrolyte Electrochemical Stability and Interfacial Structure. *Acc. Chem. Res.* **2017**, *50*, 2886–2894.
- (84) Keyzer, E. N.; Matthews, P. D.; Liu, Z.; Bond, A. D.; Grey, C. P.; Wright, D. S. Electrochemically active species in aluminum electrodeposition baths of AlCl₃/glyme solutions. *Chem. Commun.* **2017**, *53*, 4573.
- (85) Shakourian-Fard, M.; Kamath, G.; Sankaranarayanan, S. K. R. S. Electronic Structure Insights into the Solvation of Magnesium Ions with Cyclic and Acyclic Carbonates. *ChemPhysChem* **2015**, *16*, 3607–3617.
- (86) Angell, M.; Pan, C.-J.; Rong, Y.; Yuan, C.; Lin, M.-C.; Hwang, B.-J.; Dai, H. High Coulombic efficiency aluminum-ion battery using an AlCl₃-urea ionic liquid analog electrolyte. *Proc. Natl. Acad. Sci. U. S. A.* **2017**, *114*, 834–839.
- (87) Rumble, J. R. *CRC Handbook of Chemistry and Physics*; CRC Press, 2018.
- (88) Qian, J.; Henderson, W. A.; Xu, W.; Bhattacharya, P.; Engelhard, M.; Borodin, O.; Zhang, J.-G. High rate and stable cycling of lithium metal anode. *Nat. Commun.* **2015**, *6*, 8147–8155.
- (89) Mohazabrad, F.; Wang, F.; Li, X. Experimental Studies of Salt Concentration in Electrolyte on the Performance of Li-O₂ Batteries at Various Current Densities. *J. Electrochem. Soc.* **2016**, *163*, A2623–A2627.

(90) Camacho-Forero, L. E.; Smith, T. W.; Balbuena, P. B. Effects of High and Low Salt Concentration in Electrolytes at Lithium?Metal Anode Surfaces. *J. Phys. Chem. C* **2017**, *121*, 182–194.

(91) Ravikumar, B.; Mynam, M.; Rai, B. Effect of Salt Concentration on Properties of Lithium Ion Battery Electrolytes: A Molecular Dynamics Study. *J. Phys. Chem. C* **2018**, *122*, 8173–8181.

(92) Geng, C.; Buchholz, D.; Kim, G.-T.; Carvalho, D. V.; Zhang, H.; Chagas, L. G.; Passerini, S. Influence of Salt Concentration on the Properties of Sodium-Based Electrolytes. *Small Methods* **2018**, *122*, 1800208.

(93) Lang, S.-Y.; Xiao, R.-J.; Gu, L.; Guo, Y.-G.; Wen, R.; Wan, L.-J. Influence of Salt Concentration on the Properties of Sodium-Based Electrolytes. *J. Am. Chem. Soc.* **2018**, *140*, 8147–8155.